Research Signpost
37/661 (2) Fort P.O., Trivandrum-695 023, Kerala, India

Recent Res. Devel. Appl. Pol. Sci., 1(2002): 313-332 ISBN: 81-7736-157-0

Novel applications for high performance polymers

James A. Newell and Meghan Spence
Department of Chemical Engineering, Rowan University, Glassboro, NJ 08028 USA

Abstract

This article describes novel applications for high performance polymers as reinforcements for structural composites, as precursors for high-performance carbon fibers, and as core fibers for conversion to silicon carbide. Detailed descriptions of efforts to enhance the compressive strength of the fibers through spinning modifications, thermal treatment, and radiation are discussed, as well as attempts to better interpret recoil compressive failure data. This paper also examines the role that flaws in high performance polymer fibers play in the failure of carbon fibers made from them. Finally, this paper covers the development of a pneumatic spreading system to facilitate the conversion of high-performance polymers to ceramic fiber.

Correspondence/Reprint request: Dr. James A. Newell, Ph.D., Department of Chemical Engineering, 201 Mullica Hill Road Rowan University, Glassboro, NJ 08028 USA. E-mail: Newell@Rowan.edu

Introduction

High-Performance composite materials are exceptionally light and exhibit exceptional mechanical properties. These composites are rapidly displacing conventional metals and metallic alloys in aerospace applications. Because these advanced composites consist of more than fifty percent fiber by volume [1], considerable research has been directed toward enhancing these fibers. The leading edge of composite materials manufacture revolves around rigid-rod aramid polymers, carbon fibers, and high performance ceramic fibers including boron and silicon carbide [2]. Each class of fiber is capable of supporting significant tensile loads and possesses strength-to-weight ratios that exceed metals. Figure 1 shows specific strength versus specific modulus of several reinforcing materials.

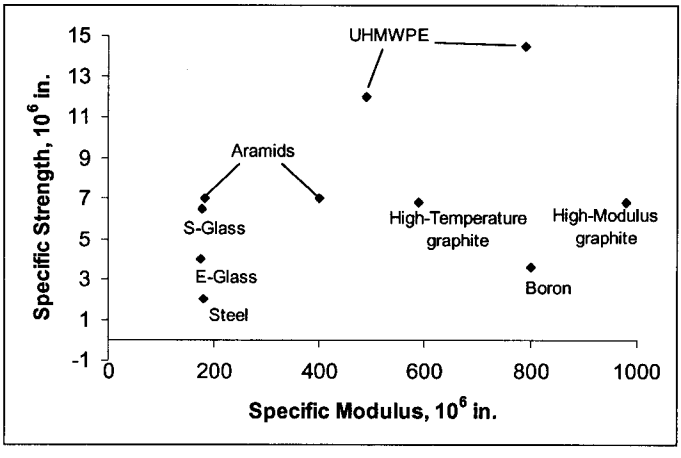

Figure 1. Specific Strengths and Moduli data of several reinforcement fibers (adapted from [3]).

High-performance polymers can serve as the reinforcement materials themselves or be used as precursor materials to carbon and ceramic fibers. The remainder of this paper describes research directed toward enhancing high-performance polymers, modeling recoil compressive failure, and making carbon and silicon carbide fibers from high performance polymers.

Enhancement of high-performance polymers

High-performance polymers such as Kevlar (poly p-phenyleneterephthalamide), shown in Figure 2, possess exceptional tensile strengths that make them ideal materials for use in such diverse products as brake pads, bullet resistant vests, kayaks, marine ropes, and tennis rackets [4]. The crystal structure of the Kevlar polymer chains can be classified as a monoclinic structure with the following lattice parameters: **a** = 7.87 angstroms, **b** = 5.18 angstroms and **c** = 12.9 angstroms with a 90° unit cell angle. In the Kevlar lattice, molecular chains exhibit two intermolecular interactions: hydrogen bonding (carbonyl oxygen to adjacent chain hydrogen(s)) acting in the **b** direction and Van der Waals dispersion forces acting in the **a** direction [5].

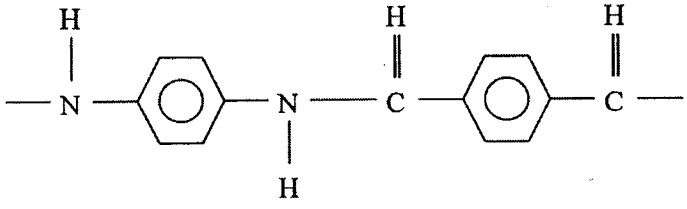

Figure 2. The repeat unit of Kevlar

Conformation of the Kevlar fiber into anything other than the "trans" conformation is sterically unfavorable. Spatially, the Kevlar polymer will always strive for the most linear conformation, as shown in Figure 3 [6]. Thus, the Kevlar fiber assumes nearly perfect "stiff/rigid rod" geometry with very little branching or bending. It is this near-perfect linearity property that allows the load to be evenly distributed along the fiber, allowing a large tensile stress to be applied to these polymers. In addition to the near-perfect linearity, weak transaxial forces between polymers strands also contribute to high performance polymers superior tensile strength as shown in Figure 4 [7].

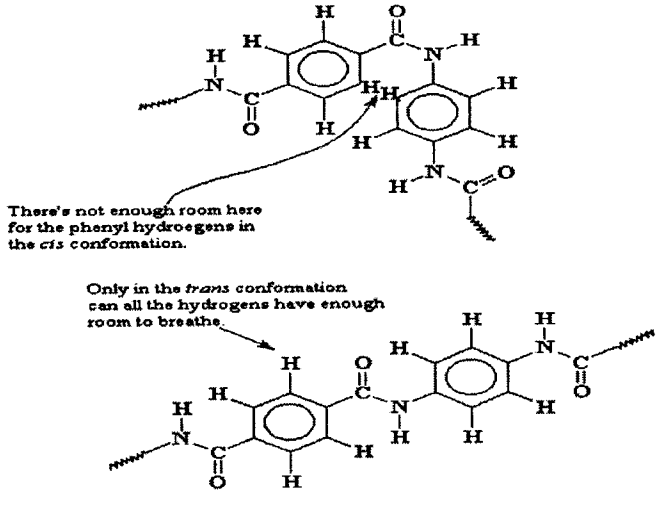

Figure 3. Stereochemical implications of the Structure of Kevlar

Kevlar exhibits a compressive-to-tensile strength ratio of between 0.13 and 0.25 [8]. This obviously puts Kevlar at a disadvantage for compressive applications. Despite this limitation, Kevlar still has one of the higher compressive strengths of the high-performance polymers [8]. Generally, this has been attributed to its interchain network of hydrogen bonds. Balluff [9] presented a discussion of this network and its reduction of the degrees of freedom in the material. This reduction dramatically alters the deformation for rigid rod networks.

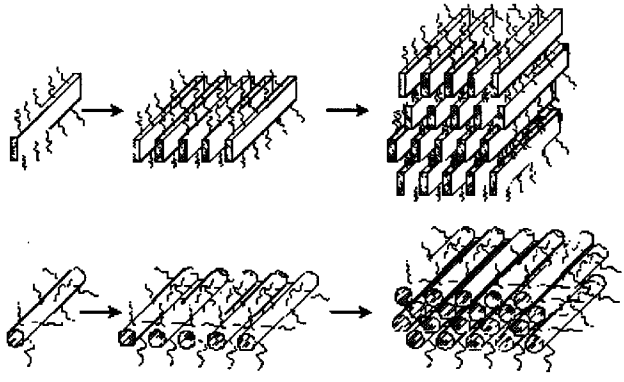

Figure 4. Representations of the "rigid-rod" linearity in High Performance Polymers (7)

Two distinct strategies exist to enhance the compressive strength of rigid rod polymers. Some groups have investigated introducing a crosslinking agent during spinning. Sweeny [10] used an active aryl halide on the polymer units themselves. Once exposed to heat treatment, the halogen is eliminated and a free-radical is formed. Once this initiation takes place, adjacent molecules of the polymer may react and cross-link. The resultant prefiber was comprised of both PPTA and halogenated aryl moeties. The extruded, halogen-bearing polymer was then subjected to various temperatures for various durations in order to develop aryl free-radicals. The aryl radicals would then facilitate the formation of crosslinks via a ring-coupling phenomenon. The degree of crosslinking could be quantified as a function of percentage of polymeric halide retained. Sweeny *et al.* recognized that a high degree of crosslinking could not be accommodated without affecting the interchain hydrogen bonding. Moreover, it was concluded that the crystal structure of Kevlar will not accommodate a high level of crosslinking.

Jiang *et al.* [11] developed an activated form of PPTA by incorporating XTA, a benzocyclobutene-modified derivative of terepthalic acid, into the polymer backbone during prefiber production. Various concentrations of the XTA were spun into the Kevlar fibers during the dry-jet wet spinning stage of the production process in order to control the degree of crosslinking. The XTA was triggered into reactive status via heat treatment at temperatures within the range of 325 and 425 °C. Summarily, the XTA-rich PPTA fibers appeared to exhibit crosslinking as verified by swelling assays. Accordingly, recoil tests showed a slight improvement in the compressive strength of these modified Kevlar fibers, accompanied by a decrement in tenacity.

Although these studies provide insight into the crosslinking mechanisms, any commercially viable enhancement of rigid-rod polymers will have to result from post-spinning treatment of the as-spun fiber. Sweeney [6] *et al.* examined the influence of heat treatments in a nitrogen atmosphere on the mechanical properties of Kevlar-29. They utilized a fractional factorial experimental design to examine the influence of the treatment temperature, ramp rate (rate of temperature increase of the furnace that is heat treating the Kevlar-29 fiber), and the soak time (duration of time that the Kevlar-29 fiber is subjected to the maximum treatment temperature). Figures 5-7 show the primary findings of this study.

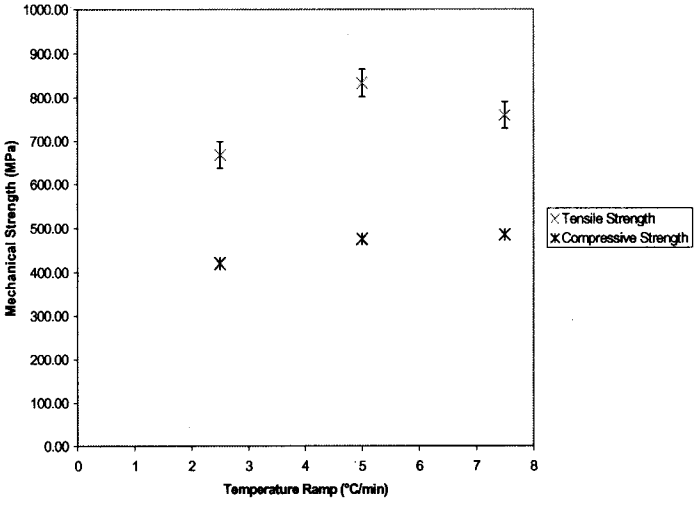

Figure 5. Maximum Treatment Temperature Dependence of Mechanical Properties

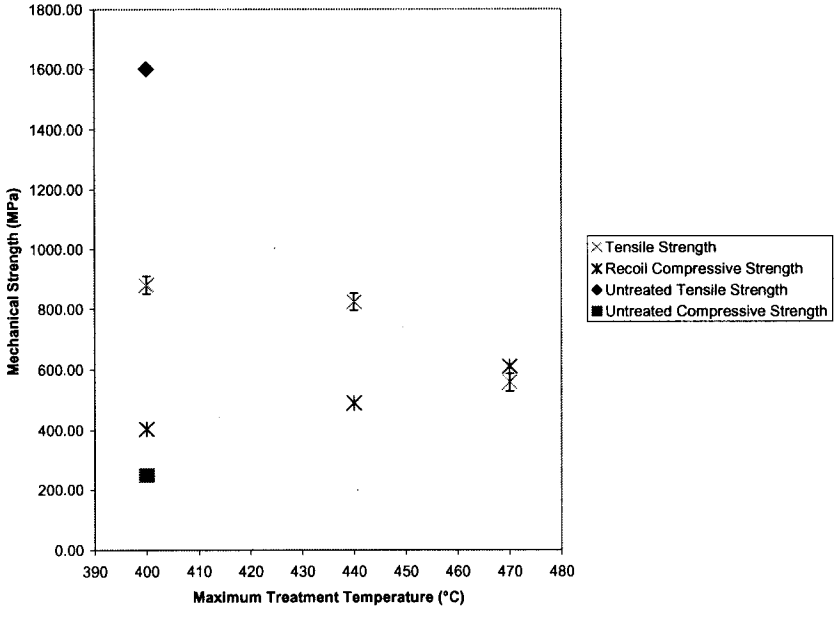

Figure 6. Dependence of Mechanical Properties on Temperature Ramp

There are clear manifestations of alteration of the Kevlar fiber at the molecular level in the mechanical properties of thermally treated Kevlar-29 polymer. This thermally induced change effects a loss in linearity of the PPTA polymer. The loss in linearity, at

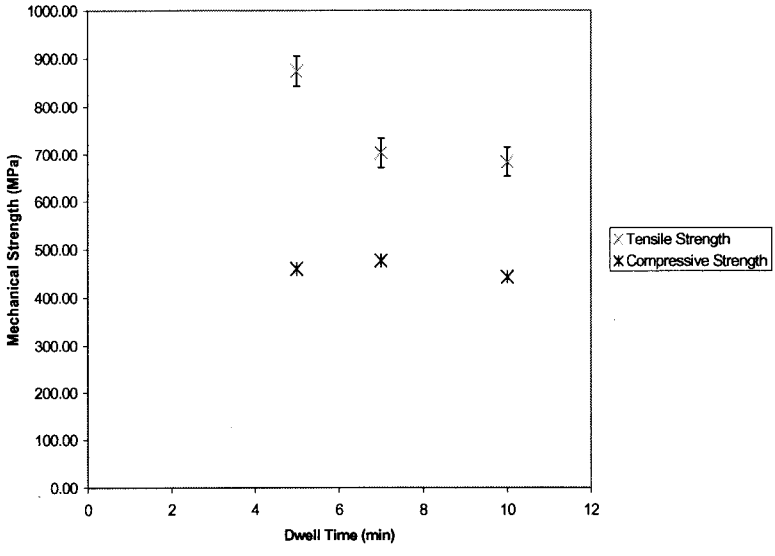

Figure 7. Dwell Time Dependence of Mechanical Properties

the macroscopic level, shows itself in the form of tensile strength degradation and compressive strength enhancement. The experimental series has determined that treatment temperature plays a key and prominent role in both the loss in tensile strength and gain in compressive strength. Furthermore, it was shown that temperature treatment ramp and treatment soak time hold some type of effect over the tensile property degradation of the PPTA polymer.

Another experiment dealing with the enhancement of Kevlar-29 compressibility was performed using electron beam (E-Beam) radiation. E-Beam radiation offers several potential advantages over thermal processing of polymers. These advantages include ambient temperature processing, improved material compatibilities and reduced treatment times [12]. Woods and Pikaev [13] have demonstrated that exposing organic substances to high-energy radiation leads to the formation of reactive free-radical species, similar to those formed in the Sweeny study. This radiation polymerization has been described in detail by several researchers [14-16].

One mechanism capable of generating such radiation is through the use of high-powered electron accelerators such as AECL's IMPELAs (Industrial Processing Linear Accelerators) in the energy range above 5 MeV [17,18]. Newell, Puzianowski, and Schmidt [19] irradiated Kevlar-29 samples using the AECL I-10/1 electron accelerator at Acsion [20]. This device is shown in Figure 8. Each fiber batch was exposed in air for three seconds to radiation levels of 0 (as a control), 100, 500, 1000, and 1100 kGy. The single filament testing procedure used in this study followed the procedure described in ASTM Standard D-3379-75 [21].

Table 1 shows that E-Beam radiation increases the recoil compressive strength of Kevlar-29 fibers with greater increases in recoil compressive strength corresponding to

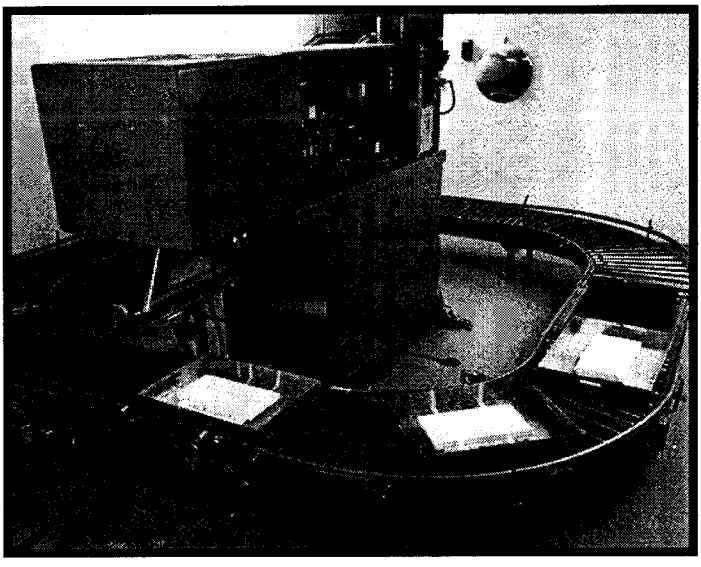

Figure 8. Acsion Industries I10/1 Electron Accelerator

Table 1. Tensile and Compressive Strengths of E-Beam treated Kevlar-29 Fibers [19]

Radiation Level (kGy)	Mean Tensile Strength (MPa)	Mean Recoil Compressive Strength (MPa)
0	2160 ± 63	365 ± 6
100	2043 ± 120	368 ± 8
200	1996 ± 86	381 ± 9
500	1891 ± 71	404 ± 8
1000	1786 ± 93	472 ± 7
1100	1723 ± 87	487 ± 7

exposure to higher radiation levels. Increases in excess of 33% were found for the highest treatment level analyzed. Concurrently, E-Beam radiation results in a decrease in the tensile strength of the fiber, but only by 20% in even the highest radiation level tested. Still, it is clear from these data that there is a significant decrease in the tensile strength of Kevlar fibers with increasing radiation. The free-radical reaction induced by the radiation would likely result in partial crosslinking of the fibers, which would disrupt the linear structure. This disruption should decrease the tensile strength while increasing the capacity of the fiber to distribute a compressive load. Finally, this study showed that a nearly linear inverse relationship exists between the gains in recoil compressive strength and the losses in tensile strength, as shown in Figure 9.

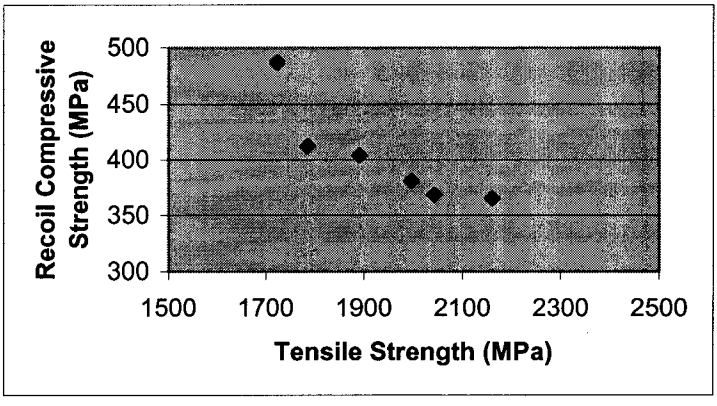

Figure 9. Recoil Compressive Strength versus Tensile Strength for E-Beam Treated Kevlar [19]

Interpretation of recoil compressive failure data

It is generally accepted that the compressive failure in high performance fiber reinforced composites results from the low compressive strengths of the fibers [22-24]. Therefore, accurate and simple measurement of compressive failure data in fibers is essential. Compressive testing of composites is well established by ASTM [25], but these tests involve many steps and large quantities of fiber. Therefore, it would be advantageous to directly measure the compressive strengths of the fibers themselves. At least four different test procedures exist to estimate the compressive strength of fibers. These tests include the bend test, the elastic loop test, testing based on a single filament imbedded in a matrix, and the recoil test. For polymeric fibers, the fiber compressive strengths estimated from composite compression tests agree most accurately with those obtained by the recoil test [8].

The recoil test is conceptually simple. Fibers are placed under a static tensile load. Next, the fiber is ruptured using either an electric discharge or surgical scissors. The stored energy travels down both halves of the fiber in the form of a recoil compressive wave. The two fiber halves either survive this recoil wave or they experience a secondary failure. Figure 10 depicts recoil compressive failures and survivals. This analysis makes several assumptions [26] about the fiber. Specifically, the fiber obeys Hook's law for linearly elastic materials, is rigidly clamped at each end, has no initial velocity, and has a uniform initial stress along its length at failure. From these assumptions, the axial stress history following tensile failure can be represented by the solution of the Fourier series shown in Equation (1),

$$\frac{\sigma(x,t)}{\sigma_0} = \sum_{m=0}^{\infty} \frac{4}{(2m+1)\pi} \sin\frac{(2m+1)\pi}{2} \cos\frac{(2m+1)\pi x}{2L} \cos\frac{(2m+1)(E/\rho)^{0.5} t}{2L} \qquad (1)$$

where x is the fiber coordinate from a clamped end, σ/σ_0 is the normalized stress, L is the length of the broken fiber end, m is an integer between zero and infinity, t is time, E is Young's modulus, and ρ is density.

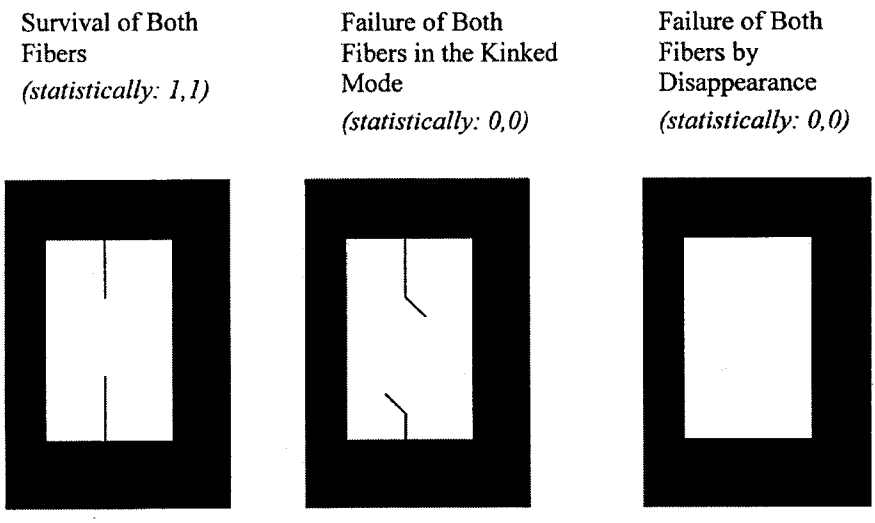

Figure 10. Visual Depiction of Fiber Survival and Failure after Recoil Compressive Testing

During the recoil, each half of the cut fiber will experience the same relaxation and compressive stresses. Thus, each test will lead to two data points (the top and bottom halves of the fiber). However, the actual compressive strength of a tested filament cannot be determined directly using the recoil test. Because failure is artificially induced, the resulting recoil compressive wave may be significantly above or significantly below the intrinsic compressive strength of the fiber. If the fiber ends experience a secondary failure, there is no way to ascertain how much stress above the intrinsic compressive strength the recoil wave imparted on the fiber. Similarly, there is no way to know how much the intrinsic compressive strength of the fiber exceeded the stress imposed by the recoil compressive wave that resulted in two survivals.

Several methods have been proposed to evaluate recoil test data. These methods fall in to two distinct categories. The first method used by Allen [26], Wang et al. [27], and Crasto and Kumar [28] arranges the data in order of ascending load levels. A stress range is identified over which the data change from all survivals to all failures. The mean of the two endpoints of this range is presented as the average recoil compressive strength of the fiber set. In essence, this approach disregards the majority of data points and characterizes the compressive properties of the entire fiber batch based on two points. Additionally, the next fiber tested always could radically change the estimated mean strength if it were to become the highest survivor or lowest failure.

The second approach, developed by Hayes [29], is to gather large quantities of recoil compression data and apply a Weibull model to characterize the underlying distribution. Hayes estimated the average recoil compressive (σ_{rc}) strength as

$$\sigma_{rc} = \sigma_0 \Gamma\left(1+\frac{1}{M}\right) \tag{2}$$

where σ_0 and m are the Weibull scale and shape parameters, respectively, and Γ is the statistical Gamma function. Although the Hayes method provided a reasonable fit of recoil failure data, the large amount of data required to accurately characterize a single sample makes this method impractical for widespread application.

Newell and Gustafson [30] propose the use of a moving average method. This method starts with the random election of an arbitrary stress level. After the recoil compressive test is completed, an examination of the binary pair is performed. If both ends of the fiber pass, the stress level of the next test is increased by 20 MPa, similarly, if both ends of the fiber fail, the stress level in turn is decreased by 20 MPa. However, if one end of the fiber passes while the other end of the fiber fails, the test is repeated at the same stress. The incremental increase/decrease process is repeated and the mean test level is recorded as the estimate of the mean recoil compressive strength of the fiber batch, as shown in Equation (3)

$$\sigma_{rc} = \frac{\sum_{i=1}^{N} \sigma_i}{N} \tag{3}$$

where N is the number of fibers tested. Clearly, the mean test level should eventually approach the mean recoil compressive strength. If the current test level is significantly below the mean, the filament is more likely to survive, thereby raising the estimate with the next test. Conversely, if the current test level is significantly above the mean recoil strength, the filament is more likely to fail, resulting in a lower estimate. The results would be biased by the initial random guess. Therefore, only the last thirty filaments tested are used in the moving average.

A series of simulations were performed to validate the new moving-average methodology. A random number generator was used to generate simulated intrinsic recoil compressive strength data for filaments following Normal, Exponential, and Weibull distributions. The Weibull distribution was selected because it is the most likely to represent the true failure of fibers [31-33].

Once the data were obtained, comparisons between the new methodology and the Method of Allen were performed. The results of these simulations clearly indicate the advantages of the moving average method. In every case, the moving average method converged upon the true sample mean more quickly and reliably than the Method of Allen. More importantly, the new method makes it far easier to determine when the mean has been adequately characterized. The simulations of the method of Allen demonstrated the susceptibility to single statistical outliers. More importantly, the moving-average technique is less affected by statistical outliers, utilizes more of the data set, and converges more conclusively. Although the Moving Average method bases its estimate on the previous thirty trials, data from simulations after 10 and 25 trials are included in the tables. These data points show the initial biasing of the estimate caused by the random first guess. Between trial 25 and 50, the effects of this biasing disappear. Table 2 shows the results of 100 simulation runs performed on simulated Weibull distrubtion failure data.

Table 2. Results of Method of Allen and Moving Average Method Applied to Simulated Weibull Distributed Failure Data (σ_{rc} = 400 MPa) [30]
(Average of 100 simulations)

Number of Fibers	Method of Allen	Moving Average Method
	Number of Times the estimated σ_{rc} fell within 5% of the true value	Number of Times the estimated σ_{rc} fell within 5% of the true value
10	52	44
25	57	50
50	66	78
75	67	84
100	72	88
125	74	90
150	77	92
175	79	94
200	80	94

Carbon fibers from high performance polymers

Carbon fibers possess exceptional tensile properties and substantially better compressive strengths than high-performance polymers, but are generally too expensive for most high volume applications [34]. Their high cost is a direct result of the lengthy, multistep process needed to convert existing precursor materials into high-performance carbon fibers. Polyacrlyonitrile (PAN) currently serves as the precursor to over 90% of all commercial carbon fibers. PAN, like other commercial precursors, requires an oxidative stabilization process in which the fiber is converted to a thermally stable ladder polymer that will not melt when exposed to the high temperatures needed for carbonization [35-37].

Newell *et al.* [38] have shown that poly p-phenylene benzobisoxazole (PBO) fibers can be converted directly to carbon fibers without stabilization, which dramatically reduces the cost of processing and allows for continous (rather than batch) processing. The structure of PBO is shown in Figure 11. However, the use of PBO-based carbon fibers is limited by their substandard tensile strength. Table 3 compares properties of commercial PAN-based, mesophase pitch-based and PBO-based carbon fibers.

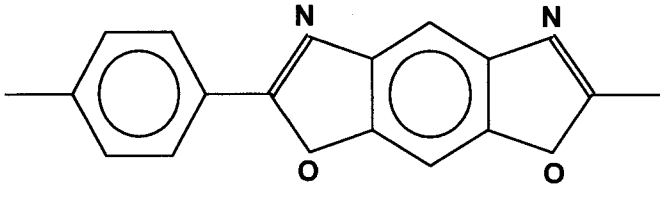

Figure 11. The Repeat Unit of PBO

Table 3. Properties of Carbon Fibers [39]

Precursor Material	Product Designation	Tensile Strength (GPa)	Tensile Modulus (GPa)	Electrical Resistivity (μΩ-m)
PAN	T-300	3.65	231	18
Pitch	P-55	1.90	415	9
PBO	Batch-1400	0.73	180	11
PBO	Cont.-1400	1.05	175	14
PBO	Batch – 1800	0.52	245	13
PBO	Cont. - 1800	0.85	183	10

Newell and Edie [39] were able to show that the nitrogen bound in the oxazole ring of the PBO fibers is released at elevated temperatures and disrupts the developing crystalline structure of the carbon fibers. Similar behavior has been described in the literature for the high temperature release of sulfur from mesophase pitch-based fibers [40].

Observation and quantification of the role of flaws in the precursor material is not as direct. Microscopic flaws cause tensile failure below the intrinsic strength of the fiber [41]. Therefore, analysis of tensile failure data can be used to gain insight into the distribution of flaws within the fiber. Tensile data do not conform to a rigid statistical distribution, therefore cannot be accurate represented by a fixed statistical distribution. The Weibull distribution is preferred for analyzing tensile data [41]. The Weibull cumulative distribution function takes the form:

$$F_i = 1 - \exp(\frac{\sigma}{\sigma_o})^m \tag{4}$$

where F_i is the probability of a given link failing at or below a given stress level, σ is the applied stress level, σ_o is a scale factor which represents the severity of flaws and m is the shape factor which relates to the distribution of flaws. If the fiber is viewed as a chain of interlocking links, the probability of the fibers survival (S_i) for any link can be written as:

$$S_i = 1 - F_i \tag{5}$$

If any of the individual links fail, the entire fiber will fail. Therefore, the probability of survival for a fiber of gauge length (L) is the product of the survival probabilities for each link in that length of fiber.

$$S = \prod_{i=1}^{L} S_i \tag{6}$$

The assumption that each link fails or survives independently of its neighbors and that the strength of each link can be represented by a single Weibull distribution enables Equation (6) to be rewritten as:

$$S = (S_i)^L \tag{7}$$

or

$$S = \exp(-L(\frac{\sigma}{\sigma_o})^m) \tag{8}$$

Because the fiber must survive or fail, the probability of failure at a given stress level is written as:

$$F = 1 - \exp(-l(\frac{\sigma}{\sigma_o})^m) \tag{9}$$

This represents the Equation for a Simple Weibull Model. However, Newell and Edie showed that the simple Weibull model does not provide an adequate representation of tensile failure data. Instead, a model accounting for artificial failures that result from the testing method must be considered.

During a tensile test, fibers are mounted to a testing tab with epoxy. The atypical stress distribution at the fiber/resin interface has been shown to result in some fraction of observed failures [42]. These failures would be independent of the gauge length of the sample tested. If both microscopic flaws and end effects led to independent failures, the Weibull model would become

$$F = 1 - \exp(-L(\frac{\sigma}{\sigma_{o1}})^{m1}) \exp(-(\frac{\sigma}{\sigma_{oE}})^{m_E}) \tag{10}$$

Newell and Edie showed that the end effect model provided an exceptional fit of the tensile failure data. More significantly, the model also showed that the shape factors representing failure by true flaws was statistically indistinguishable for the PBO-based carbon fibers and the precursor fibers from which they were made. This implies that the flaw distribution present in the precursor fiber was the same as that in the carbonized fiber. If this is the case, the damage associated with nitrogen release only exacerbated the existing flaws and improvements in the spinning process will be essential for PBO-based carbon fibers to become commercially viable.

Newell and Sagendorf [43] also showed that the end effect Weibull model could be used as a predictor of tensile failure at gauge lengths outside the range of model calibration. In this study, as-received Kevlar-29 fibers were tensile tested at gauge lengths of 10, 25, and 40 mm. The resulting failure data were used to determine four empirical constants using a maximum likelihood regression. The model and parameters were used to predict failure frequency at a gauge length outside the initial range (5 mm), as shown in Figure 12.

The reaction kinetics of the carbonization and graphitization of PBO fibers have also been examined [44]. Unlike most polymeric fibers, the unique molecular structure of PBO enables the unstabilized fiber to develop to some long range order at temperatures above 1600°C. Initially, these fibers consist of highly disordered or turbostratic sheets of aromatic molecules. Eventually, relatively ordered graphene planes develop within

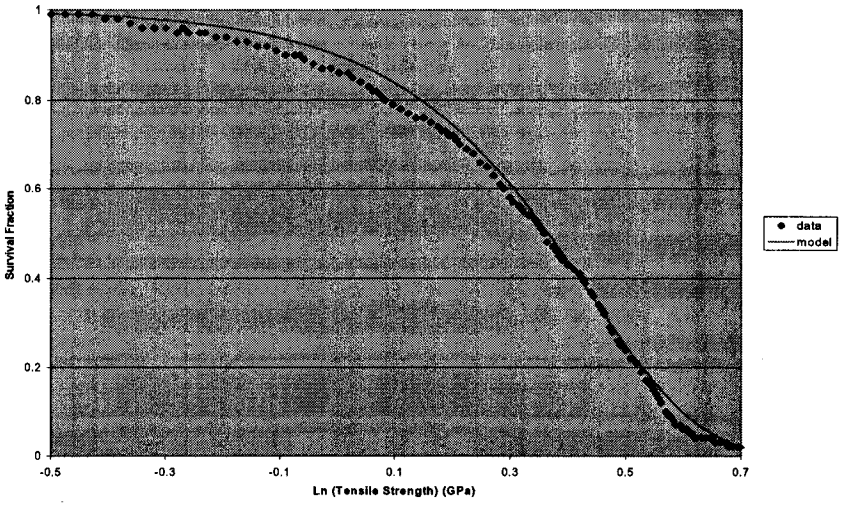

Figure 12. Comparsion of the End-Effect Weibull Model with Tensile Failure Data at a 5-mm Gauge Length

the fibers. As the fiber becomes more ordered, the mean interplanar spacing should become closer to the 3.35 angstroms associated with crystalline graphite and the size of the ordered region, the stack height (Lc), should increase.

Crystallite growth is a kinetic phenomenon that can be represented by the classical Arrhenius equation of the form

$$\frac{d\,L_C}{dt} = k_0 \exp(\frac{-E_A}{RT}) \tag{11}$$

where L_c is the crystallite size or stack height, dt is the change in time, k_0 is the pre-exponential constant, E_A is the activation energy of the graphitization process, R is the gas constant, and T is the absolute temperature. Equation (11) can be rewritten as

$$\ln(\frac{dL_c}{dt}) = \ln(k_0) - \frac{E_A}{RT} \tag{12}$$

From this form, the activation energy can be determined from a plot of ln (dL_c/dT) versus 1/T.

Newell *et al.* found an activiation energy of 120 $\pm$ 17 kcal/mol for the crystallite growth. Typical activation energies for the graphitization of other precursor materials have been reported to range from 100 to 250 kcal/mol [1,45,46].

Newell *et al.* [44] also showed that the carbonization of PBO fiber could be modeled as a free radical polymerization consisting of initiation, propagation and termination steps as shown below:

$$P \rightarrow R\bullet \qquad \text{(Initiation)}$$

$$R\bullet + P \rightarrow R\bullet \qquad \text{(Propagation)}$$

$$R\bullet + R\bullet \rightarrow C \qquad \text{(Termination)}$$

where P is a PBO molecule, R• is a molecular fragment containing a free radical and C is a carbonized molecule.

Determining the appropriate kinetic constants for the proposed reaction sequence is relatively straightforward. Because no external initiator is needed and the monomer pool is essentially infinite, the initiation reaction can be considered to be of zero order. The transient nature of free radicals prevents the concentration [R•] from being measured directly. However, some boundary approximations can be made. At the onset of initiation, the concentration of free radicals is small, so the initiation rate can be assumed to be much greater than the termination rate. Therefore, the reaction can be represented by the equation

$$K\frac{dM}{dt} = k_{I_0}\exp(-\frac{E_A}{RT}) \tag{13}$$

Initial mass loss data was obtained from isothermal TGA (thermogravimetirc analysis) trials. An activation energy of 76 $\pm$ 6 kcal/mol was determined for the thermal initiation of free radicals. This is comparable to the activation energy of petroleum pitch feed stocks, which are reported to vary between 43 and 98 kcal/mol [47].

High performance polymers as silicon carbide precursors

As Table 4 shows, silicon carbide fibers possess tensile and compressive properties comparable with high performance carbon fibers, but with significant oxidation resistance. Thus, continuous fiber ceramic composites can function in high temperature oxidative environments without experiencing the brittleness associated with traditional ceramics [2].

Table 4. Properties of High-Performance Fibers [48]

Material	Tensile Strength (GPA)	Tensile Modulus (GPa)	Compressive Strength (GPa)
Kevlar-29	3.5	125	0.39 – 0.48
PBO	5.7	306	0.20 – 0.40
Toray M60J Carbon Fiber	3.8	585	1.67
ARC Trimarc I Silicon Carbide	3.4	460	1.55 – 1.75

The experimental challenge is to produce these high-performance silicon carbide fibers reliably and at a low cost. Currently, most commercial silicon carbide fibers are produced by coating a suitable substrate using a chemical vapor deposition (CVD) process. The use of silicon carbide coatings is not new. Mesophase pitch fibers have long been coated as a barrier to oxidation [49]. Tungsten wire, the most common substrate in silicon carbide manufacture, is expensive and has a rough surface that is not ideal for the deposition process. An optimal silicon carbide precursor would possess the following four characteristics:

- a smooth surface with a uniform diameter
- a low coefficient of thermal expansion compatible with that of silicon carbide
- sufficient tensile strength to withstand the coating process
- a low cost

An ideal solution to this would be to use a low cost, low modulus carbon fiber substrate [50]. Carbon fibers made from high-performance polymers provide a viable alternative. Kevlar can be carbonized without oxidative stabilization to form fibers with diameters of approximately 7 microns, moduli of less than 150 GPa, and tensile strengths of approximately 1 GPa [48]. During the CVD process, each fiber must be unencumbered by its neighbors long enough to avoid fiber bridging. Newell and Puzianowski [48] developed a pneumatic spreading system to achieve this spreading.

A fiber spreading towline, shown in Figure 13, was constructed. As-received Kevlar fiber was passed through a carbonization furnace and pinched between rubberized rollers to allow enough slack to be maintained in the line for spreading to occur. Another pinch roller was located beyond the last spreader before the traversing waywinder. The towline design principles were similar to those used in a continuous fiber coating system developed by Lackey [51], but the Lackey spreader was designed for the coating of a continuous monofilament and did not need to address spreading issues.

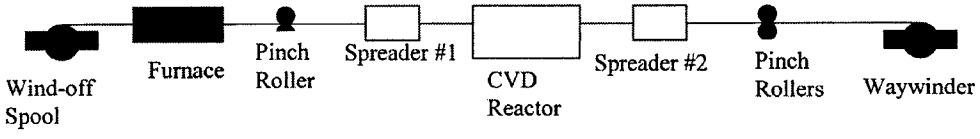

Figure 13. Towline Configuration

A series of spreaders that focused on axial spreading effects was found to be the most effective. First, the tow was passed through an Axial Venturi Type I spreader, shown in Figure 14. In this spreader, the inner channel widens, much like the nozzle of a Venturi flow meter. The resultant Venturi effect aligns the streamlines of the spreading gas favorably. The divergent nozzle moves the tow through the pressure differential as described by the Bernoulli equation, resulting in a highly chaotic motion of filaments within the tow. At the same time, the venturi throat minimizes the formation of unwanted vortices and eddies. Although this spreader alone provides a reasonably effective short-duration spreading, a second spreader is required to maintain adequate

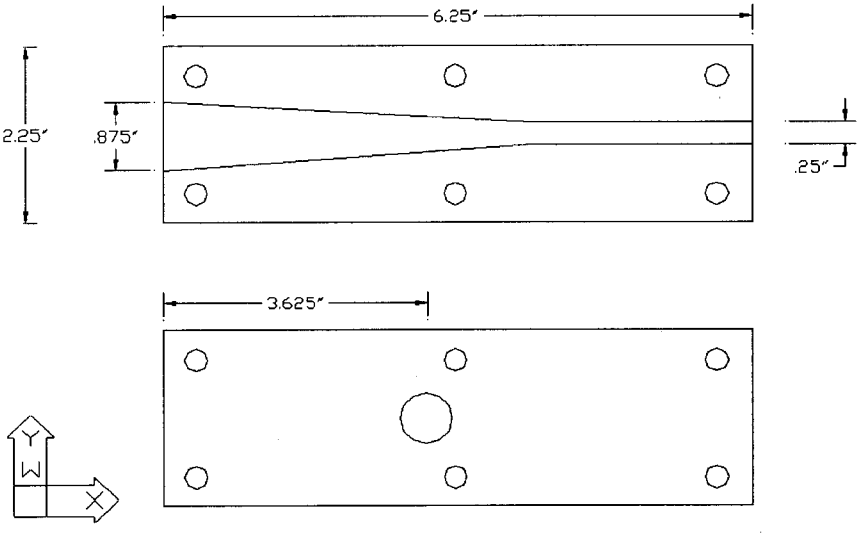

Figure 14. Design of Axial Venturi Type I Spreader [48]

separation between filaments for sufficient time to allow coating without bridging between adjacent filaments.

At the opposite end of the spreading region, the tow is passed through a type II Axial Venturi spreader, as shown in Figure 15. This spreader looks very much like the Axial Type I spreader with some further innovations. The location of the gas inlet instead of being in the middle of the spreader is located at the rear of the spreader. The tow is feed through a narrow hole drilled at a 30° angle to the channel. It was believed that the abrupt forcing of the gas at a narrow right angle into the channel caused a significant pressure loss

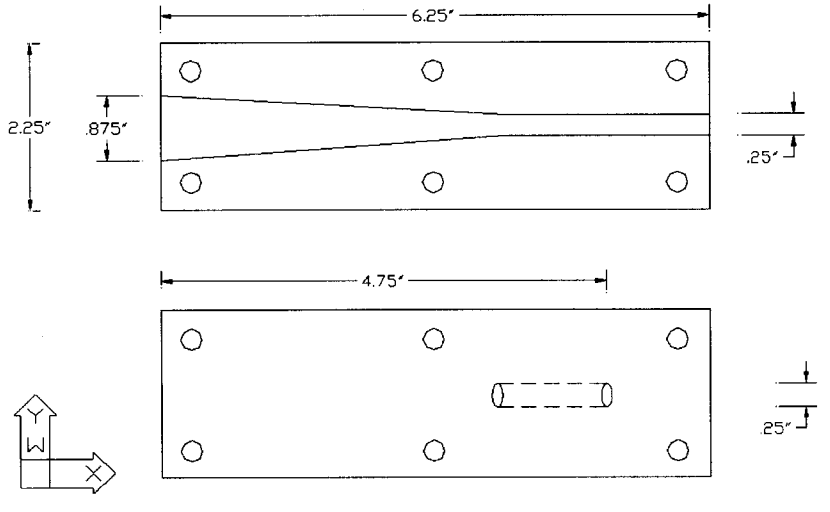

Figure 15. Design of Axial Venturi Type II Spreader [48]

in the axial type I spreader. With the gas being fed at the end of the spreader this could be avoided. In this design, the entire gas flow could be biased to one end of the spreader only. Using this system of pinch rollers and Venturi spreaders in series, a highly chaotic, three-dimensional spread was achieved and maintained through a linear distance of three feet. With gas velocities of 25 cfm (12 cm^3/s), a spread with a total diameter of 3-4 inches was maintained across the entire three feet. Figures 16 and 17 show this spreading.

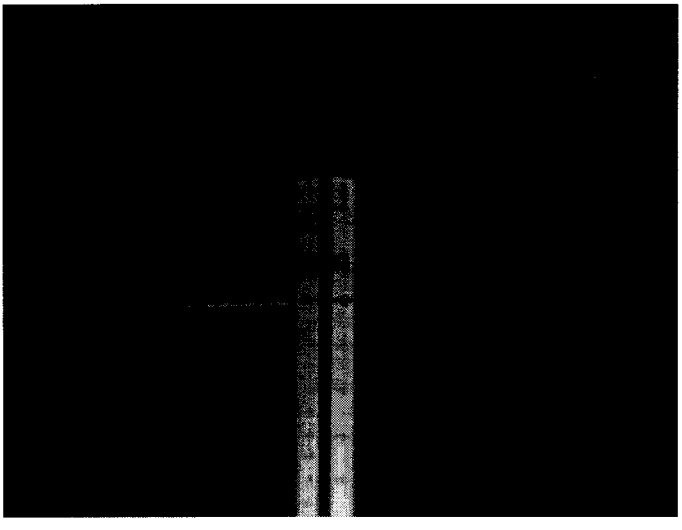

Figure 16. Photograph of Unspread Kevlar Fiber

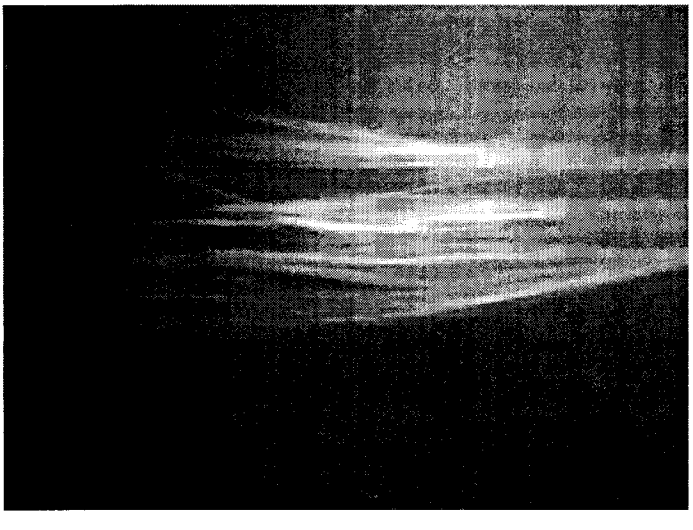

Figure 17. High Speed Photo of Kevlar During Spreading

Conclusion

This paper has summarized advances in the development of novel uses of high performance polymers. Rigid rod polymers are limited by their relatively poor compressive strength, but this strength has been improved through thermal treatment and electron beam radiation. Improvements have been made to the interpretation of recoil compressive failure data to enable improved quantification of these improvements. The development of carbon fibers from unstabilized high performance polymers was examined. Detailed kinetic models of the carbonization and graphitization processes are provided, as well as consideration of the factors limiting the tensile strength of these carbon fibers. Finally, a novel spreading system was developed to facilitate the use of carbonized Kevlar as a core fiber for subsequent CCVD coating to form silicon carbide.

References

1. Fitzer, E., 1989, Carbon, 27(5), 621.
2. Chin, K. and Wessel, J., 1996, Chemical Engineering, 103(10), 80.
3. Jang, B., 1994, Advanced Polymer Composites, ASM International, Materials Park, Ohio.
4. Hattery G. R. and Hillman M., ed., 1986, High Performance Polymers, Hanser Publications, New York.
5. Liang Y, Quichen, Z., and Warner, S., 1994, Journal of Polymer Science: Part A: Polymer Chemistry, 32, 2207.
6. Sweeney, D., Newell, J., Picerno, S., and Kurzeja, T., 2002, High Performance Polymers, Accepted for Publication (2002).
7. McCarthy, T. F., Witteler, H., Pakula, T. and Wegner, G., 1995, Macromolecules, 28, 8350.
8. Kumar, S. and Helminiak, T. E., 1990, SAMPE Journal, 26(2), 51.
9. Ballauff, M., 1989, Angew Chem. Adv. Materials, 28(8/9), 135.
10. Sweeny, W., 1992, Journal of Polymer Science: Part A: Polymer Chemistry, 30, 1111.
11. Jiang, T., Rigney, J., Jones, M., Markoski, L., Spilman, G., Mielewski, D. and Martin, D., 1995, Macromolecules, 28, 3301.
12. Singh. A., Saunders, C., Lopata, V., Kremers, W., and Chung, M., 1995, Proceedings of the International Conference on Composite Materials and Energy, 389.
13. Woods, R. J. and Pikaev, A. K., 1994, Applied Radiation Chemistry: Radiation Processing John Wiley and Sons, New York.
14. Chapiro, A., 1962, Radiation Chemistry of Polymeric Systems, Interscience, New York.
15. Charlesby, A., 1960, Atomic Radiation and Polymers, Pergamon Press, Oxford.
16. Wilson, J. E., 1974, Radiation Chemistry of Monomers, Polymers and Plastics, Marcel Dekker, New York.
17. McKeown, J., Labrie, J. P., and Funk, L. W., 1985, Nuclear Inst. and Meth., B10/11, 846.
18. McKeown J., 1985, IEEE Trans. Nucl. Sci., NS-32, 3292.
19. Newell, J. A., Puzianowski, A. A., and Schmidt, L. R., 2002, High Performance Polymers, Accepted for Publication.
20. Barnard, J. W. and Stanley, F. W., 1989, Nucl. Instrum. Methods Phys. Res., B40/41, 1158.
21. ASTM Standard D3379-75 (reapproved 1989).
22. Greenwood, J. M. and Rose, P. G., 1974, Journal of Materials Science, 9(11), 1809.
23. Newell, J. A., 1994, The Conversion of Poly p-Phenylene Benzobisoxazole (PBO) to Carbon Fiber, Ph.D. Dissertation, Clemson University.
24. Kulkarni, S. V., Rice, J. S., and Rosen, W. B., 1975, Composites, 6(5), 217.
25. ASTM Standards D695 and D3410.

26. Allen, S. R., 1987, Journal of Materials Science, 22, 853.
27. Wang, C. S., Bai, S. J., and Rice, B. P., 1989, Proceedings of the American Chemical Society, Division of Polymeric Materials: Science and Engineering, 61, 550.
28. Crasto, A. S. and Kumar, S., 1990, SAMPE Proceedings, 35, 318.
29. Hayes G. J., 1993, Analysis of the Single Filament Recoil Test, Ph.D. Disseration, Clemson University.
30. Newell, J. A., and Gustafson, J. M., 2001, High Performance Polymers, 13, 251.
31. Newell, J. A., and Sagendorf, M. T., 1999, High Performance Polymers 11, 197.
32. Wagner, H. D., Phoenix, S. L., and Schwartz, P., 1984, Journal of Composite Materials, 18, 312.
33. Alsoun, E. M., Donnet, J. B., Guilpain, G., Nardin, M., and Schultz, J., 1989, Journal of Materials Science, 24, 3504.
34. Glatz, J. G., Kinna, M. A., Riley, W. C., 1988, DOD Metal Matrix Composites Information Analysis Center, Current Highlights, 8, 1.
35. Pinghua, W., Jie, L., Zhongren, Y., and Rengyuan, L., 1992, Carbon, 30(1), 113.
36. Dunham, M. G. and Edie, D. D., 1992, Carbon, 30(3), 435.
37. Mathur, R. B., Bahl, O.P., and Mittal, J., 1992, Carbon, 30(4), 657.
38. Newell, J. A., Rogers, D. K., Edie, D. D., and Fain, C. C., 1994, Carbon, 32(4), 651.
39. Newell, J.A. and Edie, D. D., 1996, Carbon, 34(5), 551.
40. Rogers, D. K., Jones, S. P., Fain, C. C., and Edie, D. D., Carbon, 31, 303.
41. Johnson, D. J., 1987, Chemistry and Physics of Carbon, 20, 1.
42. Stoner, E. G., Edie, D. D., and Dunham, M. G., 1994, Journal of Materials Science, 29, 6561.
43. Newell, J. A. and Sagendorf, M. T., 1999, High Performance Polymers, 11, 197.
44. Newell, J. A., Edie, D. D., and Fuller, Jr., E. L., 1996, Journal of Applied Polymer Science, 60, 825.
45. Fischbach, D. B., 1971, Chemistry and Physics of Carbon, 7, 1.
46. Fitzer, E. and Weisenberg, S., 1976, Carbon, 14, 323.
47. Newman, B. A., 1986, in Carbon '86: Proceedings of the Annual Conference on Carbon, Pergamon, New York, 147.
48. Newell, J. A. and Puzianowski, A. A., 1999, High Performance Polymers, 11, 197.
49. Emig, G., Popovska, N. and Schoch, G., 1993, Thin Solid Films, 241, 361.
50. Fitzer, E., Kehr, D., Morin, D. and Sahebkar, M., 1975, Proceedings of the Fifth International Conference on Chemical Vapor Deposition, 623.